University Library



A gateway to Melbourne's research publications

Minerva Access is the Institutional Repository of The University of Melbourne

Author/s:
Hutchins, N;Monty, JP;Hultmark, M;Smits, AJ

Title:
A direct measure of the frequency response of hot-wire anemometers: temporal resolution issues in wall-bounded turbulence

Date:
2015-11-22

Citation:
Hutchins, N., Monty, J. P., Hultmark, M. & Smits, A. J. (2015). A direct measure of the frequency response of hot-wire anemometers: temporal resolution issues in wall-bounded turbulence. Experiments in Fluids, 56 (1), https://doi.org/10.1007/s00348-014-1856-8.

Persistent Link:
https://hdl.handle.net/11343/283317

Experiments in Fluids manuscript No.
(will be inserted by the editor)

A direct measure of the frequency response of hot-wire anemometers.

Temporal resolution issues in wall-bounded turbulence

N. Hutchins · J. P. Monty · M. Hultmark · A. J. Smits

Received: date / Accepted: date

Abstract Based on the need to characterise the accuracy of hot-wire anemometry (HWA) in high Reynolds number wall-bounded turbulence, we here propose a novel direct method for testing the frequency response of various systems to very high frequency velocity fluctuations (up to 50 kHz). A fully developed turbulent pipe flow is exploited to provide the input velocity perturbations. Utilising the unique capabilities of the Princeton Superpipe it is possible to explore a variety of turbulent pipe flows at matched Reynolds numbers, but with turbulent energy in different frequency ranges. Assuming Reynolds number similarity, any differences between the appropriately scaled energy spectra for these flows should be indicative of measurement error. Having established the accuracy of this testing procedure, the response of several anemometer and probe combinations are tested. While these tests do not provide a direct or definitive comparison between different anemometers (owing to non-optimal tuning in each case), they do provide useful examples of potential frequency responses that could be encountered in HWA experiments. These results are subsequently used to predict error arising from HWA response for measurements in wall-bounded turbulent flows. For current technology, based on the results obtained here, the frequency response of under- or over-damped HWA systems can only be considered approximately flat up to $5-7$ kHz. For flows with substantial turbulent energy in frequencies above this range, errors in measured turbulence quantities due to temporal resolution are increasingly likely.

N. Hutchins · J. P. Monty
Department of Mechanical Engineering
University of Melbourne, Parkville, VIC 3010 Australia
E-mail: nhu@unimelb.edu

M. Hultmark · A. J. Smits
Department of Mechanical and Aerospace Engineering
Princeton University, Princeton, NJ 08544, USA

Keywords temporal resolution · hot-wire anemometry · frequency response

1 Introduction

There has been a concerted push over the last few decades towards higher Reynolds number facilities for studying wall-bounded turbulence. For example: the Princeton Superpipe (Morrison et al, 2004); the NDF at IIT Chicago (Hites, 1997); the MTL at KTH Stockholm (Österlund, 1999); the HRNBLWT at the University of Melbourne (Nickels et al, 2007); the LLF at DNW Netherlands (Fernholz et al, 1995) and the CICLoPE at Predappio (Talamelli et al, 2009). In general, these higher Reynolds number facilities will be characterized by smaller scales of turbulence and a higher frequency content in the turbulence spectrum. Subsequently, this push to higher Reynolds numbers has reinvigorated attention to hot-wire sensor resolution. Building on the widely used results of Ligrani and Bradshaw (1987), there have been a slew of recent papers investigating spatial resolution of hot-wire sensors, with a particular emphasis on high Reynolds number wall-bounded turbulence (Hutchins et al, 2009; Chin et al, 2009, 2011; Smits et al, 2011; Örlü and Alfredsson, 2010; Monkewitz et al, 2010; Segalini et al, 2011a,b). However, during this same period, the temporal resolution (or dynamic response) of the HWA system has received considerably less attention (see Ashok et al 2012 for a recent attempt to consider both the effects of temporal and spatial resolution in grid generated turbulence).

There are two principal techniques that may be employed to determine the temporal response of a HWA system, both of which involve introducing some form of known perturbation into the system and measuring the response of the anemometer's output signal. For *direct* methods, this perturbation is introduced as a velocity fluctuation into the

flow in which the hot-wire probe is measuring. Such methods are attractively straight-forward, unequivocally providing a direct measure of the system response to a velocity impulse (which is, after all, what we wish to know). However, the need to accurately impose high frequency velocity perturbations on to a flow poses numerous experimental challenges (attempts at direct methods will be discussed below). In the absence of readily available convenient direct methods, the majority of users rely on *electronic* testing to estimate the system frequency response. The standard procedure involves injecting a square-wave or sine-wave perturbation into the bridge and observing the response of the anemometer's output signal. For most anemometers there is typically some user-defined control of the square-wave response such that an 'optimum' response can be obtained (via adjustment of the bridge damping and inductance). The 'optimum' square-wave response is described by Freymuth (1977) as one in which there is a slight undershoot (of approximately 15% of the maximum). Freymuth (1977) suggests that the cut-off frequency f_c of the system can be calculated from,

$$f_c = \frac{1}{1.3\tau_c} \tag{1}$$

where τ_c is the time from the start of the square-wave input to the point where the response has decayed to 3% of its maximum value (see Bruun, 1995, for a good description of this). In applying equation (1) it is often overlooked that Freymuth (1977) defined this for the -3dB cut-off. That is, based on the above equation, one would expect a 50% attenuation in HWA measured energy at frequency f_c (and for the under-damped systems suggested as 'optimum', this 50% attenuation would be accompanied by substantial over representation of energy at lower frequencies). Bruun (1995) acknowledges this short-coming, recommending a sine-wave test for situations where a truly flat response is required. (see Oxlade et al 2012 for a recent application of this technique). Nonetheless, equation (1), or some related form, is often used to estimate the system response, with the subsequently determined cut-off frequency f_c often cited to evidence a systems ability to resolve the particular flow under investigation. Though there are numerous theoretical studies suggesting that the square-wave test can provide a reliable indication of the true response of HWA systems to a velocity impulse (e.g. Freymuth 1977), there are also a few notable exceptions in the literature highlighting cases where electronic testing seems less reliable. Hutchins et al (2009) and Valente and Vassilicos (2011), both seem to suggest that in certain situations the true temporal response of HWA systems can be substantially slower than that indicated from electronic testing (even when the response appears to conform to optimally-damped second order behaviour, Watmuff, 1995). In a review of hot-wire anemometry, Comte-Bellot (1976) notes, when discussing the electronic testing of dynamic response, that 'direct checks using flow perturbations are worth making'.

There are some notable examples in the literature where direct methods have been attempted. Khoo et al (1995) placed a hot-wire sensor in the cavity between two discs, one of which had radially machined recesses and could be rotated. This apparatus was capable of imposing known flow perturbations onto the sensor. From these experiments, it was concluded that their HWA system (Dantec 56C01) could faithfully respond up to the 1600 Hz perturbations that this experimental apparatus was capable of producing. Ko and Ho (1977) used an audio speaker to superimpose a plane acoustic wave onto the flow through a pipe. This enabled them to test the response of a hot-wire sensor within the pipe flow at frequencies up to 8 kHz. From these experiments, they concluded that their system exhibited a flat response (to within ± 3 dB) for $0.14 < f < 8$ kHz. Perry and Morrison (1970) placed a hot-wire sensor in the periodic vortex street shed from a cylinder. Using this technique, they were able to test the dynamic response of their system at frequencies up to approximately 10 kHz. They found that their in-house system was flat up to approximately 8 kHz, while the tested Disa 55A01 anemometer exhibited a 3dB attenuation at 6 kHz. In this case both directly measured responses were found to closely match those predicted from electronic square-wave testing. A further variant of direct testing are those experiments that have sought to test the frequency response of the HWA system by rapid cyclical heating of the hot-wire sensor element. As an early example, Kidron (1966) heated the sensor element (operated in constant current mode) using modulated microwaves. Bonnet and de Roquefort (1980) used a modulated laser to heat the sensor (operated in constant temperature mode), finding good agreement with electrical sine-wave testing.

For this study, based on the need to investigate the accuracy of hot-wire anemometers in high Reynolds number turbulent boundary layers, we aim to pursue a direct method for testing the dynamic response of a HWA system to very high frequency velocity fluctuations (up to 50 kHz). To achieve this we will use a turbulent wall-bounded flow itself to provide the input velocity perturbations.

2 Rationale

The assumption of Reynolds number similarity states that two fully-developed turbulent pipe-flows with differing characteristic velocity, lengthscale and kinematic viscosity, yet the same Reynolds number, must be identical in all appropriately scaled statistics. We here exploit this assumption to vary the frequency content of the turbulent spectrum in order to investigate the frequency response of hot-wire anemometers.

Although the idea of this set of measurements is very simple, the execution is possible only because of the unique capabilities of the Princeton Superpipe (Zagarola and Smits, 1998; Smits and Zagarola, 2005). By pressurising the entire pipe flow facility up to 220 atm, the kinematic viscosity of the working fluid (air) can be altered by a factor of more than 100. This capability is primarily motivated by the desire to operate at very high Reynolds numbers (without experiencing compressibility effects), however, we here exploit this unique feature to test multiple turbulent pipe flows, all at matched Reynolds numbers, but with vastly differing centerline velocities (and thus vastly differing frequency content).

The most convenient Reynolds number for fully turbulent pipe flow is the friction Reynolds number or Kármán number, defined as,

$$Re_\tau = \frac{U_\tau R}{\nu} \tag{2}$$

where U_τ is the friction velocity, ν is kinematic viscosity and R is the pipe radius. For a given facility, the radius R is fixed, and Re_τ is typically altered by changing the centerline velocity (which will alter U_τ). In the case of the Superpipe, we also have the option of altering ν.

In the lower part of a turbulent boundary layer, we know that the smallest scales of turbulence have a size that can be expressed in terms of the viscous length-scale ν/U_τ. We also know that (close to the wall) these smallest scales will convect at a speed that approximately scales on U_τ. Therefore the small-scale turbulent energy will have a frequency observed by a stationary observer that will scale as,

$$f \propto \frac{U_\tau^2}{\nu} \tag{3}$$

In fact Hutchins et al (2009) have shown over a range of Reynolds numbers that the highest frequencies in a turbulent boundary layer are fixed at,

$$f_m \approx \frac{U_\tau^2}{3\nu} \tag{4}$$

Comparing equations (2) and (3) we note that Reynolds number scales on U_τ/ν, while the maximum frequency in the flow scales on U_τ^2/ν. Consider 2 experiments conducted in the Superpipe: Experiment 1 is performed at a given centerline velocity U_0 and ν. For experiment 2, if we now halve the friction velocity U_τ (by halving the centerline velocity), and halve the kinematic viscosity ν (by increasing the pressure), the Reynolds number will remain the same, but the frequency content of the flow will be reduced by a factor of 2 (f will be halved according to equation 3). In other words the viscous lengthscale (the ratio ν/U_τ) remains unaltered between experiment 1 and 2, but the viscous timescale has been altered. Consider a hot-wire probe, inserted into a fully developed turbulent pipe flow at a fixed distance z from the wall for both experiments. The single-normal hot-wire probe has a sensor length l and diameter d. In terms of key experimental parameters, the viscous scaled wall-normal position z^+ ($= zU_\tau/\nu$) for the fixed probe will not change between experiments with matched Re_τ. In addition the viscous scaled sensor length l^+, will also remain constant and thus there will be no variation in the spatial resolution of the probe (Ligrani and Bradshaw, 1987; Hutchins et al, 2009). Thus all experimental conditions will remain unchanged other than the frequency content of the turbulence. Based on the assumption of Reynolds number similarity, any differences between the spectral content of the two measured signals, can therefore only be attributed to the frequency response of the anemometry system. This simple idea forms the basis of the measurements performed here.

This idea also implicitly relies on the notion that the heat transfer from the wire is primarily a function only of Reynolds number. The equation for the heat transfer from the wire, and thus the voltage output from the anemometer, is strictly a function of Reynolds number and Prandtl number (Bruun, 1995; Li et al, 2004). However, since in this case the Reynolds number is held constant, and since the Prandtl number is only a very weak function of pressure (Li et al, 2004), one might expect the mean output voltage from the anemometer to be relatively invariant across the five experiments described above. This assumption is important, since the stability of the system is directly related to the mean cooling of the wire. For the experiments listed below (experiments $e1$ to $e5$ in table 1, which range from a pressurisation of 2.5 atm up to 22 atm) the variation in mean output voltage is less than one standard deviation of the fluctuating voltage measured at $z^+ = 80$. This variation in mean voltage (and hence heat transfer) is equivalent to a change in mean velocity of $\approx 7\%$ of the centerline velocity U_0, indicating that the effective cooling or heat transfer from the sensor, and thus the stability of the system, is almost invariant for these constant Reynolds number experiments. (Appendix A indicates that such small changes in mean heat transfer are unlikely to substantially alter the stability of the system).

3 Experiments

3.1 Anemometery and probes

In total three different anemometers were tested. These are referred to throughout as CTA1, CTA2 and CTA3. We make no claims here to have explored the entire performance space for each anemometer, nor do we claim that the systems tested are optimally damped or optimally configured. The reported behaviour will be specific to the particular configurations selected here and, as such, a different user may attain different performance. For these reasons, we have chosen

e	pressure (kPa)	ν ($\times 10^6$) (m^2s^{-1})	U_0 (ms^{-1})	U_τ (ms^{-1})	Re_τ	z (mm)	z^+	l (mm)	l^+	probe	$f^+ = 0.01$ (kHz)
1	249	6.24	27.0	1.00	10385	0.5	80.3	0.5	80.3	55P15	1.61
2	329	4.73	20.5	0.76	10391	0.5	80.3	0.5	80.3	55P15	1.22
3	459	3.39	14.7	0.55	10395	0.5	80.4	0.5	80.4	55P15	0.88
4	758	2.05	8.9	0.33	10401	0.5	80.4	0.5	80.4	55P15	0.53
5	2156	0.72	3.1	0.12	10383	0.5	80.3	0.5	80.3	55P15	0.19

Table 1 Experimental parameters for the 5 matched cases with CTA1

not to name the anemometer systems. The purpose of these experiments is to provide a test of the direct response of the system to velocity perturbations, which may then serve as a comparison with the more widely applied standard electronic test.

Two probe types were investigated. For the majority of measurements, a slightly modified Dantec 55P15 boundary-type probe was used, with prong spacing 1.5 mm. Wollaston wires are soldered to the prong tips and etched to produce a 2.5μm diameter platinum sensing element of length 0.5 mm. The un-etched portion (or stubs), which are 0.5 mm in length, have an estimated diameter of 40 μm. These probes are operated with an overheat ratio of 1.8 yielding a mean wire temperature of approximately 240°C. The in-house Princeton Nano-scale Thermal Anemometery Probe (NSTAP) was also tested, with a platinum sensor of length 60μm (see Kunkel et al, 2006; Bailey et al, 2010; Vallikivi et al, 2011, for full details). The NSTAP was operated with an overheat ratio of 1.3 yielding a mean wire temperature of approximately 210°C.

3.2 Experimental Conditions

Based on the notion that Re_τ would be held constant, we also know that the ratio,

$$S = \frac{U_0}{U_\tau}, \tag{5}$$

would remain unchanged. The first step in these measurements was to approximately determine the value S for the Reynolds number at which we would be conducting experiments. The static pressure drop was measured in the initial unpressurised case to determine skin friction, yielding a value of $S = 27$ for $Re_\tau \approx 10000$[1]. The Superpipe, was pressurised from approximately 2.5 atm up to approximately 22 atm over a typical series of 5 experiments. For each pressure, the centerline velocity is carefully adjusted such that the ratio U_0/ν (and thus the viscous length-scale ν/U_τ) is held constant. Table 1 shows experimental conditions for the test of CTA1. The table is loosely divided into sections. The first group of parameters demonstrate that by careful adjustment of the Superpipe pressurisation and the centerline velocity, the same Re_τ can be attained for a range of centerline velocities ranging from $3-27$ ms^{-1}. The variation in Re_τ is less than 0.3%. The second group of parameters reassure that key experimental parameters z^+ (the wall-normal position of the probe) and l^+ are virtually unaltered. The final column shows the frequency associated with $f^+ = 0.01$, which is the approximate non-dimensional frequency corresponding to the near-wall turbulent energetic peak due to the near-wall cycle (see for example Hutchins et al, 2009). It is clear that this set of matched experiments will have different frequency content in the turbulent spectra (the frequency content is shifted by almost an order of magnitude).

Hot-wire signals for all experiments were sampled at 300kHz using a Data Translation DT9832 16bit analogue-to-digital converter (ADC). The ADC has an input range of ±10V, giving a bit resolution of ≈ 0.3 mV (the standard deviation of the sampled output from the anemometer is approximately 1V). Hutchins et al (2009) estimate that energy in turbulent boundary layers is negligible for $t^+ < 3$. The sampling rate of 300 kHz corresponds to $\Delta t^+ \approx 0.07 - 0.5$ for these experiments. Since the sampling frequency sufficiently exceeds the maximum frequency content of the turbulent energy, the Nyquist criterion is met. Hence aliasing will not be an issue and analogue filters are not employed. To guarantee equivalent convergence in energy spectra, the sample length T was nominally fixed at 37000 boundary layer turnover times ($TU_0/r = 37000$). Thus T increased from 120 seconds for experiment 1 to approximately 1000 seconds for experiment 5.

The particular set of experiments detailed in table 1 were conducted with the probe at approximately 80 wall units from the wall. For later experiments the probe was moved closer to the wall. Figure 1 shows the pre-multiplied energy spectra ($f\Phi_{EE}$, where Φ_{EE} is the energy spectrum of the voltage fluctuations) for the 5 experiments. Note that these spectra are based on uncalibrated voltage signals. There are some noise spikes present in the raw spectra at consistent frequencies for all anemometers (due to noise sources in the lab). Spectra are smoothed and interpolated at these frequencies to remove these spikes. The pre-multiplied spectra are

[1] It should be noted that the precise value of S is not crucial to these experiments. An estimate is good enough. Any error in S will only slightly alter the overall Reynolds number at which we conducted the experiments (along with the z^+ and l^+ values). More importantly, the estimate of S in no way influences how well matched the experiments are in terms of Re_τ, z^+, l^+ etc.

normalised such that the area under the low frequency portion of the curve ($1000 < t^+ < 4000$) is forced to 1 for all experiments. The notation of vertical parentheses is used to denote normalised spectra (i.e. $|f\Phi_{EE}|$). This normalisation bypasses the need for probe calibration, thus avoiding all experimental uncertainty introduced by hot-wire drift. Perry and Li (1990) have demonstrated that uncalibrated voltage signals can give an accurate representation of the true velocity spectra. Measurement error aside, Reynolds number similarity insists that all appropriately scaled spectra should be identical. The only additional assumption relied on here is that the large-scale measured energy (the low frequency content) will be immune to the temporal resolution issues of the anemometer.

4 Results

4.1 CTA1

All data presented here are for the standard probe tip (55P15) at $z^+ \approx 80$. Figure 1(*a*) shows pre-multiplied energy spectra as a function of frequency for the experiments described in Table 1, demonstrating that this set of matched experiments has a widely varying frequency content. The darkest line, representing experiment 1 with the highest U_0 (and lowest pressure) has turbulent fluctuations at much higher frequencies than the other experiments (shown by the lighter shaded lines). The lowest speed experiment (exp. 5, the lightest line) will have the lowest frequency content, and thus will be the most immune to temporal resolution issues. For the purposes of this experiment, we must consider this curve as the baseline (the most 'correct' measurement), against which the other experiments are compared.

Figure 1(*b*) shows the same spectra normalised by the viscous time-scale (same data, with f^+ on the *x* axis). Non-dimensionalised in this way, the spectra seem to collapse quite well (there is of course the usual convergence issues at the low frequency end). Indeed, if temporal resolution were not a problem for the anemometer, Reynolds number similarity would suggest that all spectra should be identical. In spite of the apparent collapse in Fig. 1(*b*), a closer inspection of the higher frequency end of the spectra does show some systematic differences. Figure 1(*c*) shows a zoomed view of the area bounded by the dashed rectangle in Fig. 1(*b*). In this zoomed view we see systematic departures between the spectra. There is a very pronounced region centered around $f^+ = 0.08$ for which the higher speed flows (darker lines) record more energy than the baseline (lightest curve). There are signs that at higher f^+ this trend might reverse. There is also a less pronounced, but systematic trend centered around $f^+ = 0.015$, where the higher speed flows register reduced energy as compared to experiment 5. We know that any differences between the baseline case (experiment 5) and the other experiments must be due to temporal resolution issues. For each experiment number *e*, and at each value of f^+ we can define a difference function χ, as the fractional variation of the pre-multiplied spectra for a given experiment *e* (where $e = 1, 2, 3$ or 4) about the baseline case (experiment

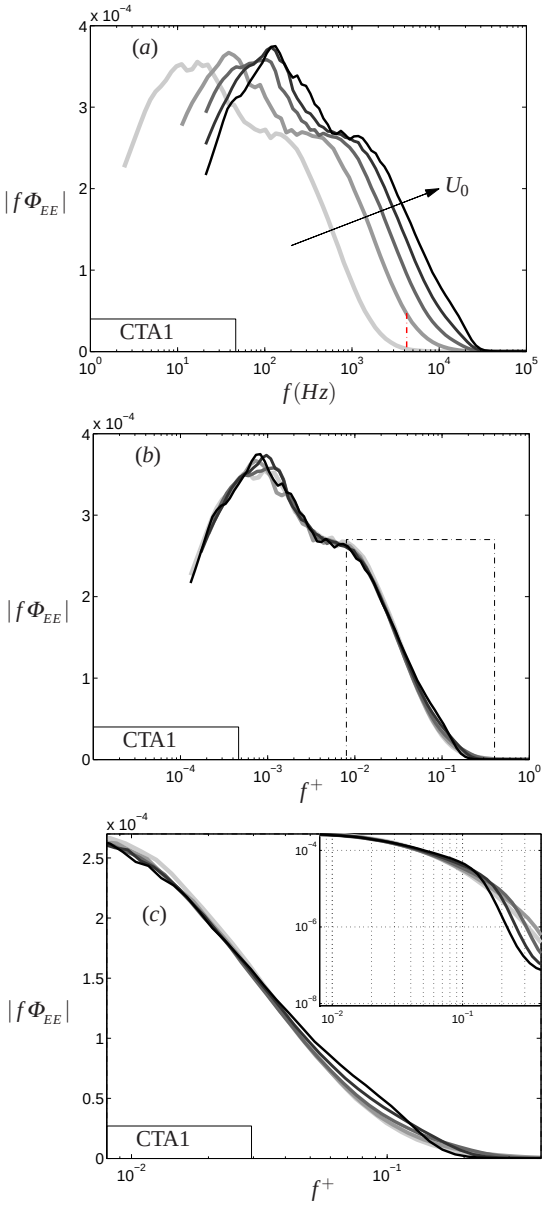


Fig. 1 Pre-multiplied energy spectra from the CTA1 experiment described in table 1 shown for (*a*) dimensional frequency in Hz, the dot-dashed vertical line represents $f_l = 1/t_l$ for case *e*5; (*b*) non-dimensional frequency f^+; (*c*) zoomed view of the region bounded by the dashed rectangle in plot (*b*). The inset in plot (*c*) shows the same zoomed view with a logarithmic ordinate. Line shading indicates centerline velocity from light (lowest U_0, $e = 5$) to dark (highest U_0, $e = 1$).

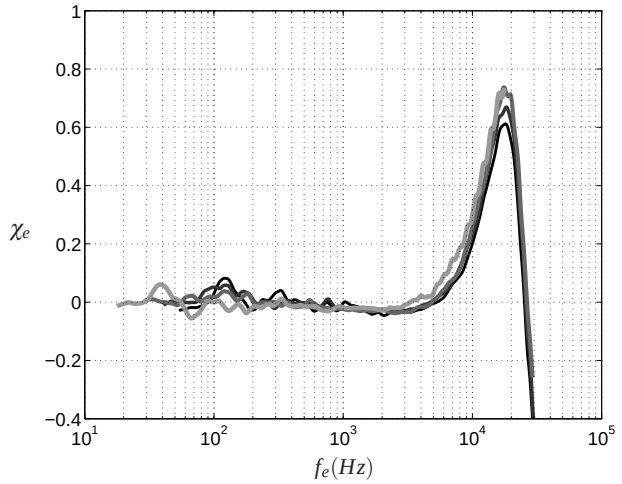


Fig. 2 The spectral difference parameter χ_e calculated for experiments $e = 1,2,3$ & 4. Line shading indicates centerline velocity from light (lowest U_0) to dark (highest U_0).

5),

$$\chi_e(f^+) = \frac{|f\phi_{EE}(f^+)|_e - |f\phi_{EE}(f^+)|_5}{|f\phi_{EE}(f^+)|_5} \quad (6)$$

So for a given experiment e, the function χ_e is a measure of the missing measured energy at each non-dimensional frequency f^+. A non-zero result for χ_e indicates that the anemometer is not accurately resolving energy at the higher frequency f_e where,

$$f_e = \frac{f^+ U_{\tau_e}^2}{\nu_e}$$

Thus, if we plot χ_e versus f_e we should obtain a measure of the attenuation due to the anemometer as a function of frequency. This is effectively a transfer function, with the input signal being the turbulent fluctuations measured in experiment 5 (the most accurate data in terms of temporal resolution) and the output signal the turbulent fluctuations measured in a higher frequency experiment e. This result is shown in figure 2 for experiments 1 to 4. The difference function χ_e is evaluated across the energetic range of turbulence for $e = 1 \rightarrow 4$ within the range $t_l^+ < t^+ < 3000$, where $1/t_l^+$ is the frequency at which the energy from the trusted signal $e5$ falls below 1% of the maximum energy (t_l^+ equals $3-4$ for the range of experiments shown here, see figure 1a). It is clear from figure 2 that the attenuation (and amplification) due to the temporal response of the anemometer system is relatively consistent across all experiments, providing confidence in the robustness of this technique. As further validation it is also noted that the same curve for χ_e can be obtained by using experiment $e4$ as the baseline (provided any attenuation inherent in the baseline is iteratively corrected for).

The curves shown for χ_e in figure 2 are relatively noisy within the range $10 < f_e < 300$ due to the general lack of convergence in the low frequency end of the spectra (as shown in figure 1a), yet seem to collapse quite well for higher frequencies. Beginning at $f_e \gtrsim 500$ Hz, there is a clear attenuation in the spectra measured by the anemometer. This attenuation peaks at approximately 4% ($\chi_e = -0.04$) in the range $1000 < f_e < 3000$. The onset of this attenuation is presumably related to the thermal inertia of the sensing element. Beyond this, at higher frequencies, we note that this trend reverses, and there is an increasing over-representation of energy beginning at frequencies in excess of $f_e \approx 5000$ Hz, and peaking at $f_e \approx 18000$ Hz. At this peak frequency, the anemometer records energy that is approximately 60 - 70 % greater than the baseline. These results would seem to indicate that quite serious systematic errors may be present in hot-wire measured data due to temporal resolution issues, in situations where the flow contains substantial energy at frequencies $\gtrsim$ 5kHz.

To reassure that the effect demonstrated by figure 2 is really a product of the anemometer frequency response and not merely an artifact of experimental technique, a further test of CTA1 was conducted in which we deliberately over-damped the square-wave response. Figure 3 shows a comparison of these two cases; the initial case (which was under-damped, as shown in the top plots) and the new case (which was over-damped, shown in the lower plots of figure 3). Both the transfer function χ_e (plots a and c) and the associated measured square-wave response (plots b and d) are shown for both damping scenarios[2]. A comparison of plots (a) and (c) demonstrates that the degree of damping does affect the behavior of χ_e, with the over-damped case exhibiting none of the resonant behaviour evident for the under-damped case. Therefore, we are confident that this experimental technique, and the parameter χ_e really is providing a measure of attenuation due to the temporal resolution of the anemometer system. The red dashed curves on figures 3(a) and (c) show the normalised energy spectra of the response of the bridge to a step input in voltage (calculated from the FFT of the square-wave response shown in plots b and d). From classical control theory, the transfer function (the Bode plot) of a linear system is obtained by taking the Fourier transform of the impulse response of a system (the impulse response can be obtained by differentiating the square wave responses shown in figure 3b and d). However, Freymuth (1967) and Weiss et al (2001) both suggest that the response of the *bridge* to a square-wave voltage input best indicates the *system* response to an impulse of veloci-

[2] The square-wave response is measured *in-situ*, with the probe at the centerline of the pipe with the centerline velocity U_0 matched to the measured mean at $z^+ = 79$ for experiment $e5$. Since the pipe has a turbulent core, the measured square-wave response is extracted from the turbulent signal using a triggered / conditional averaging technique - see Appendix B.

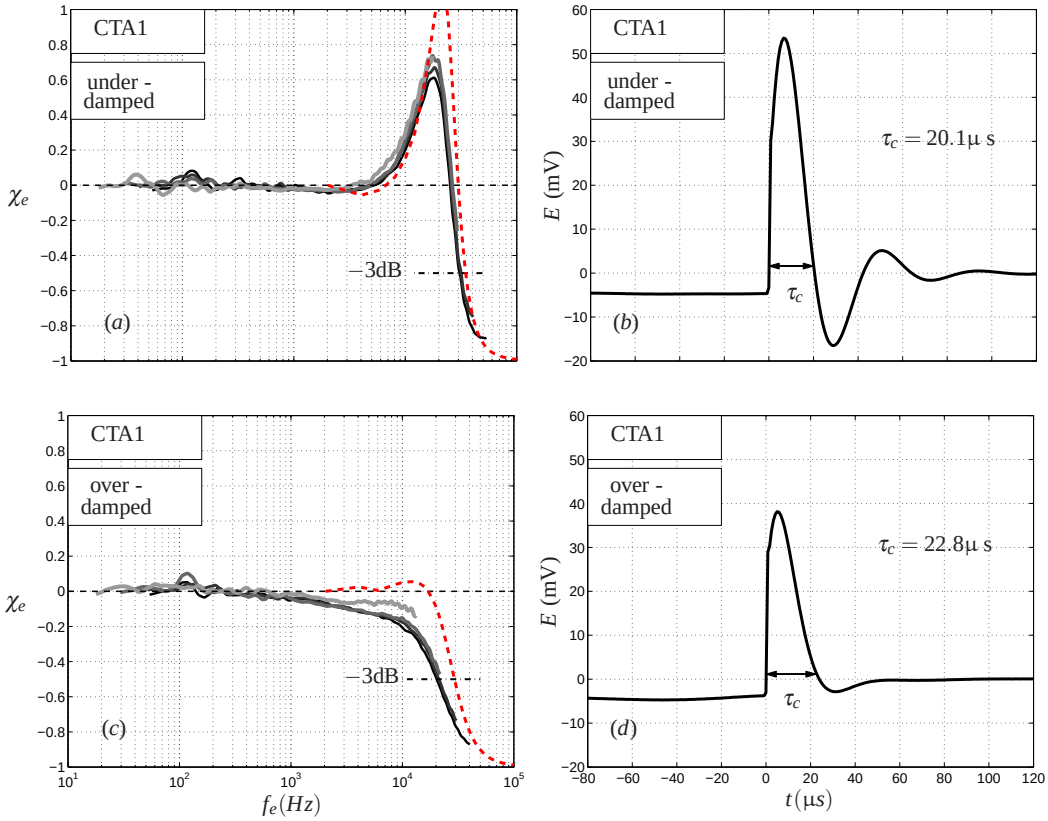


Fig. 3 The difference function (a, c) and the corresponding square wave output (b, d) for (top plots) the under-damped CTA1 and (bottom plots) the over-damped CTA1. The red dashed lines in plots (a) and (c) show the normalised Fourier transform of the square wave output. Line shading indicates centerline velocity from light (lowest U_0) to dark (highest U_0).

ty (where we define the system as the bridge plus the sensor). In the case of figure 3, the normalised energy spectra of the square wave response yields a transfer function that approximately represents the experimentally observed behaviour (though, it should be noted that the energy spectra from the square-wave response over predicts the resonant peak in figure 3*a*). Though this can only be considered an observation (based on the non-linearities of the system), the similarity is worth noting and is potentially useful. Regardless, the main purpose of figure 3 is to demonstrate that the experimentally determined transfer function χ_e is a measure of the response of the system, clearly capturing the under-damped and over-damped characteristics (shown on the top and bottom plots respectively of figure 3). It should be noted that neither response could be considered optimal. According to Bruun (1995), optimal responses are obtained when the overshoot is approximately 15% relative to the maximum of the square-wave response. For the square-wave responses shown in figure 3(c) and (d), the overshoots are approximately 30% and 8% respectively for the under- and over-damped cases. Tests of CTA2 and CTA3 (detailed below) are also non-optimal configurations, where both systems are configured with large overshoots on the square-wave response, which would be expected to lead to under-damped behaviour.

One surprising aspect highlighted in figure 3 is that relatively minor changes in the square-wave response can indicate a shift from under- to over-damped behaviour. This is of particular importance for measurements with a large range of mean velocities (such as boundary layer flows) where the response can potentially vary quite significantly between the freestream (where the mean velocity is maximum) and close to the surface (where the velocity tends to zero). This is investigated in Appendix A.

4.2 CTA2

Table 2 shows the conditions for a similar set of experiments designed to probe the frequency response of CTA2. Figure 4 shows the normalised spectra plotted against (a) dimensional and (b) non-dimensional frequency. Figure 4 (c) shows an enlarged view of the region enclosed by the dot-dashed rectangle in plot (b). In figure 4(a) there is a very clear modification in the shape of the high frequency end of

e	pressure (kPa)	ν ($\times 10^6$) (m^2s^{-1})	U_0 (ms^{-1})	U_τ (ms^{-1})	Re_τ	z (mm)	z^+	l (mm)	l^+	probe	$f^+ = 0.01$ (kHz)
0	251	6.19	27.0	1.00	10470	0.5	80.9	0.5	80.9	55P15	1.62
1	328	4.74	20.7	0.77	10470	0.5	80.9	0.5	80.9	55P15	1.24
2	457	3.40	14.8	0.55	10460	0.5	80.8	0.5	80.8	55P15	0.89
3	759	2.05	8.9	0.33	10440	0.5	80.7	0.5	80.7	55P15	0.54
4	2166	0.72	3.1	0.12	10440	0.5	80.7	0.5	80.7	55P15	0.19

Table 2 Experimental parameters for the 5 matched cases of CTA2

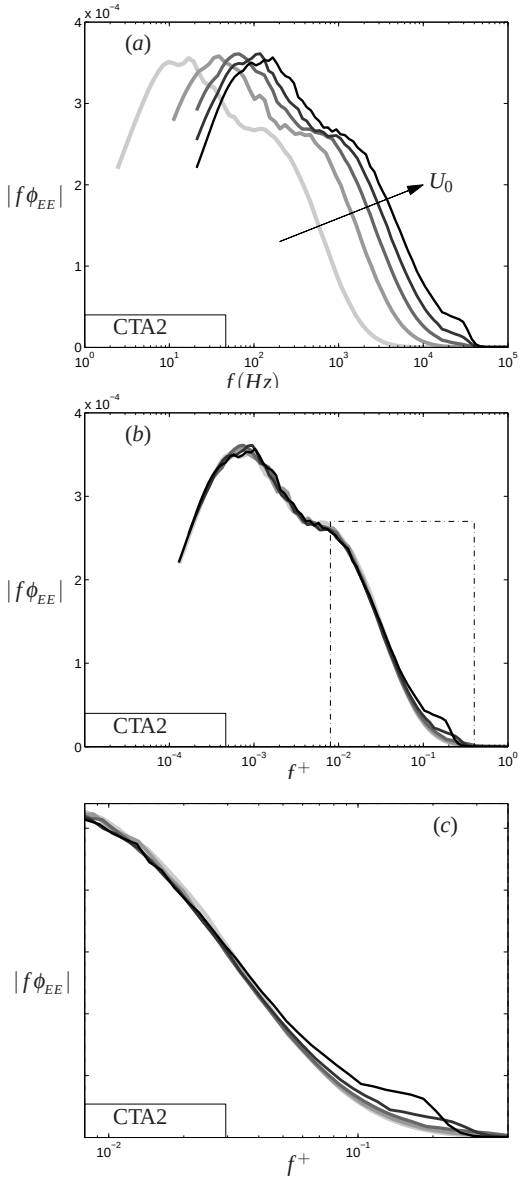


Fig. 4 Pre-multiplied energy spectra from the CTA2 experiment described in table 2 shown for (*a*) dimensional frequency in Hz; (*b*) non-dimensional frequency f^+; (*c*) zoomed view of the region bounded by the dot-dashed rectangle in plot (*b*). Line shading indicates centerline velocity from light (lowest U_0, $e = 5$) to dark (highest U_0, $e = 1$).

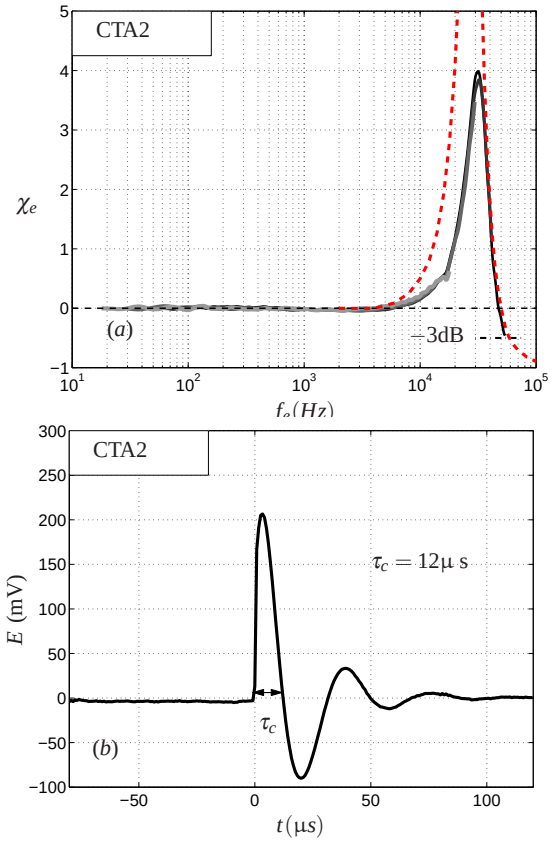


Fig. 5 The difference function (*a*) and the corresponding square wave response (*b*) for the under-damped CTA2. The red dashed line in plot (*a*) shows the normalised Fourier transform of the square wave output. Line shading on plot *a* indicates centerline velocity from light (lowest U_0) to dark (highest U_0).

the spectra, centered around $10 < f < 30$kHz. This manifests as an imperfect collapse of the non-dimensional spectra in plots *b* and *c*. In the same manner as for CTA1, the difference parameter χ_e is calculated and plotted in figure 5(a). Again the parameter χ_e is noted to collapse rather well across experiments $e = 1 - 4$. The behaviour is qualitatively similar to CTA1. There is a region of slight attenuation in the range $0.5 < f_e < 5$ kHz, peaking with $4 - 5\%$ attenuation in the range $1 < f_e < 3$ kHz. Beyond $f_e \approx 5$ kHz there is a region of very pronounced amplification of the energy peaking at $f_e \approx 31$ kHz with a gain of approximately 5 (amplification of approximately 400%). This amplification

is much greater than for CTA1. It should be noted that C-TA2 had been modified to enable compatibility with the N-STAP probe (see § 4.4). As a consequence of this modification, some of the settings were disabled which limited our ability to fine-tune the square wave response. Nonetheless, this experiment serves as a useful indication of the direct response of an anemometer tuned in this manner. Again, the transfer function χ_e can be compared to the square-wave response that was used to tune the anemometer, as shown in figure 5(b). The measured square-wave response clearly exhibits under-damped ringing behaviour which is reflected in the measured χ_e result. The normalised energy spectrum of the square wave response is shown by the red dashed line on figure 5(a). In this case, the 'Bode' plot again approximates the experimentally determined transfer function. The behavour is qualitatively similar, but the square-wave response would indicate a peak amplification of $\approx 1000\%$ occurring at $f_e \approx 28$ kHz while the experimentally determined result χ_e indicates a peak amplification of 400% at $f_e \approx 31$kHz. Based on the approximate rule given by Freymuth (1977) and reproduced here as equation (1), one can compute the -3 dB drop-off for the square-wave test from the time τ_c (≈ 12 μ s), giving $f_c \approx 64$ kHz (although the rule is based on an optimal response, which is certainly not the case for this test). The experimentally determined χ_e would indicate a -3 dB drop-off in amplitude (energy gain of 0.5 or $\chi_e = -0.5$) at a slightly lower frequency of ≈ 57 kHz. The important point to notice from the experimentally determined transfer function χ_e is that the -3 dB drop-off is not an appropriate measure for accurate measurements in wall bounded flow because,

1. The $-3dB$ drop-off is a 50% reduction in energy. Freymuth (1977) recognises this point, suggesting that a, "5% drop might be more realistic for accurate measurements", where $f_{5\%} = 1/4\tau_c$.
2. For under-damped systems, there is a resonant peak leading to substantial over representation of energy starting at frequencies that are approximately an order of magnitude lower than the -3 dB cut-off.

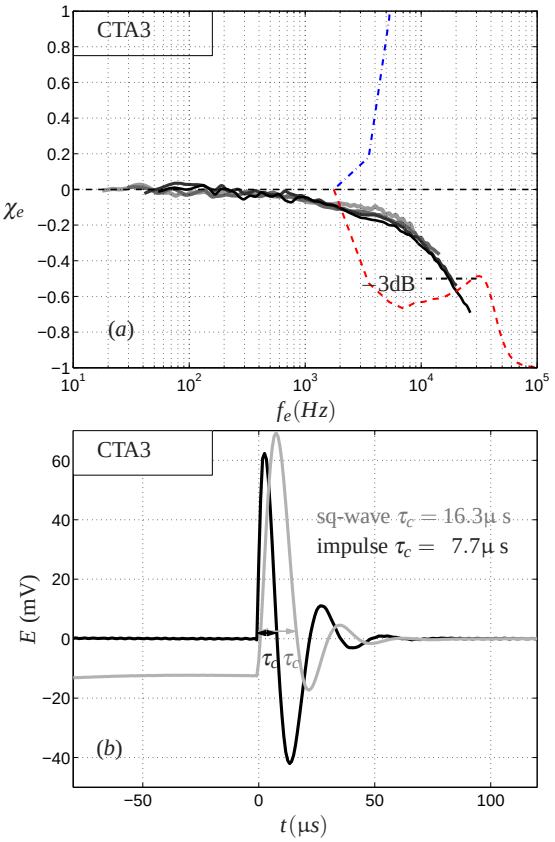


Fig. 6 (a) The difference function χ_e for CTA3 at $z^+ \approx 29$. Line shading indicates centerline velocity from light (lowest U_0, $e = 5$) to dark (highest U_0, $e = 1$). The blue dot-dashed line shows the normalised Fourier transform of the impulse test output. The red dashed curve shows the normalised Fourier transform of the integrated impulse response. (b) the corresponding (black line) impulse response (grey line) integrated impulse response.

4.3 CTA3

Table 3 lists experimental parameters for a test of CTA3. The tests were conducted in the same manner as for CTA1 and CTA2, the only difference being that these experiments were conducted at a position closer to the pipe surface, with the wire positioned at $z = 0.18$ mm ($z^+ \approx 29$). Time constraints did not permit measurements at matched z^+, however careful comparison of CTA1 and CTA2 at 2 different wall-normal positions has confirmed that the experimentally determined transfer function χ_e is relatively insensitive to changes in z^+. Figure 6(a) shows the measured temporal response for CTA3 in the near-wall position. Figure 6(b) shows the tuned frequency response indicated by an electrical pulse test. In this case CTA3 displays behaviour that is inconsistent with CTA1 and CTA. The electrical test response curve (figure 6 b) suggests that the anemometer system is noticeably under-damped, however the experimentally determined transfer function χ_e shown in plot (a) exhibits behaviour more typical of an over-damped system.

It should be noted that CTA3 has an internal impulse test (rather than the square-wave test used by CTA1 and CTA2). Freymuth (1967) and Weiss et al (2001) suggest that the response of the bridge to a square-wave voltage input best indicates the system response to an impulse of velocity. For comparison, we can attempt to recover the square-wave response from the impulse test by integrating the impulse test response, the result of which is shown in gray on figure 6(b). The electronic test results can be used to predict the cut-off frequency by measuring the time τ_c for the initial response to decay to 3% of the maximum, and using this result in equation 1. It should be noted here that equation 1 is strictly only

e	pressure (kPa)	ν ($\times 10^6$) (m^2s^{-1})	U_0 (ms^{-1})	U_τ (ms^{-1})	Re_τ	z (mm)	z^+	l (mm)	l^+	probe	$f^+ = 0.01$ (kHz)
1	250	6.18	26.8	0.99	10380	0.18	28.9	0.5	80.3	55P15	1.59
2	331	4.68	20.3	0.75	10400	0.18	28.9	0.5	80.4	55P15	1.21
3	461	3.36	14.5	0.54	10360	0.18	28.8	0.5	80.1	55P15	0.86
4	760	2.04	8.8	0.33	10360	0.18	28.8	0.5	80.1	55P15	0.52
5	2165	0.72	3.1	0.11	10320	0.18	28.7	0.5	79.8	55P15	0.18

Table 3 Experimental parameters for the 5 matched cases for CTA3

valid for optimally tuned square-wave responses (which is not the case here). However, for the impulse test, the measured τ_c indicates a cut-off frequency $f_c \approx 100$kHz. The integrated impulse would suggest that $f_c \approx 50$ kHz. These results are in contrast to the direct test shown in figure 6(a) which indicates a -3dB cut-off (where $\chi_e < -0.5$) occurs at $f_c = 17$ kHz. Hence, neither electronic test accurately conveys the measured -3dB cut-off of the system to velocity fluctuations as determined by χ_e. The blue dot-dashed and red dashed curves on figure 6(a) show the normalised energy spectrum of the impulse response and integrated impulse response respectively. Unlike the tests of CTA1 and CTA2, neither spectra seems to match the response indicated by χ_e. However, it is noted from figure 6(a) that the square-wave response gives a slightly better match to the experimentally determined performance (at least indicating an over-damped tendency). It is also worth noting that integration of the impulse is extremely sensitive to measurement accuracy.

In order to explore further the discrepancy shown in figure 6, the behaviour of the amplifier for CTA3 is investigated in figure 7(a), which shows the fluctuating voltage signal sampled from both the amplified and unamplified anemometer outputs simultaneously. An analysis of the two signals indicates that the amplifier gain is approximately 15. For comparison on the same plot both signals have been normalised by the standard deviation. The amplified signal is shown by the dashed line, and the unamplified by the solid line. Figure 7(a) suggests that the amplified signal contains less high frequency information. This is confirmed in figure 7(b) which shows the normalised premultiplied energy spectra of voltage fluctuations (spectra are normalised in the same manner as discussed in § 3.2). The filtering effect of the amplifier becomes noticeable at frequencies in excess of 1kHz, beyond which the amplified spectra (dashed curve) exhibits increasingly attenuated energy as compared to the unamplified (solid line). It should be noted that these energy spectra are for experiment $e = 1$, the highest frequency case. Thus there is already a certain degree of attenuation in these spectra owing to the temporal response of the system. Figure 7(c) shows the transfer function χ_e for both amplified and unamplified signals. Beyond $f_e \approx 2$ kHz, the degree of attenuation is increasingly worse for the amplified output. By $f_e = 10$ kHz, the amplified signal has an attenuation that is 5 times greater than the unamplified signal. In the lim-

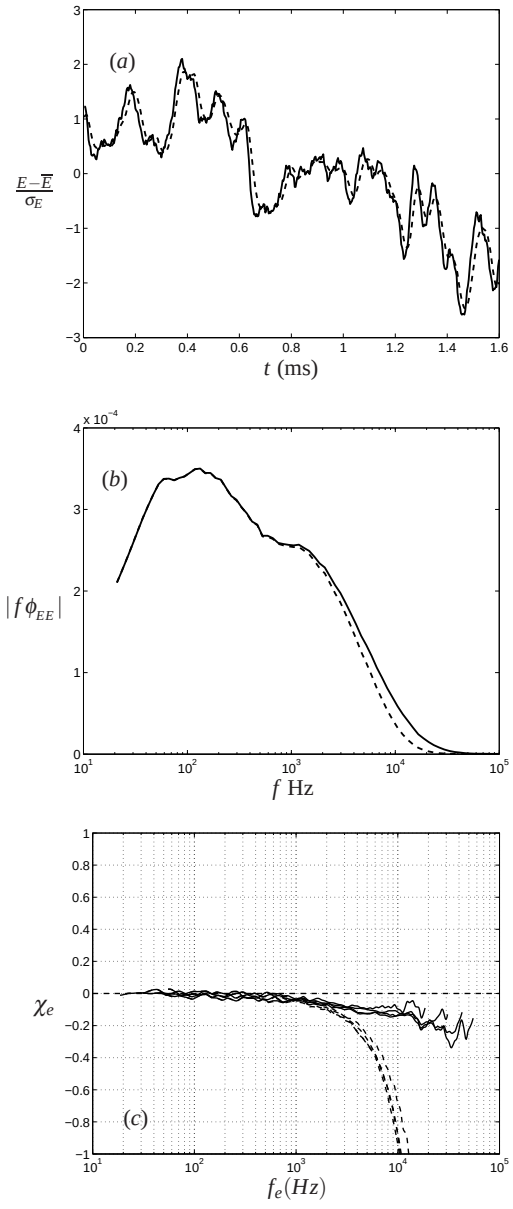


Fig. 7 Comparison of amplified and unamplified output from CTA3 at $z^+ = 80$. (a) Comparison of normalised raw fluctuating voltage signal; (b) comparison of normalised premultiplied energy spectra of streamwise velocity fluctuations; (c) Comparison of the transfer function χ_e. In all plots solid lines are the unamplified output and dashed lines are the amplified.

e	pressure (kPa)	ν (m^2s^{-1})	U_0 (ms^{-1})	U_τ (ms^{-1})	Re_τ	z (mm)	z^+	l (mm)	l^+	probe	$f^+ = 0.01$ (kHz)
1	246	6.21	26.9	1.00	10380	0.18	28.9	0.06	9.6	NSTAP	1.60
2	334	4.65	20.1	0.74	10350	0.18	28.8	0.06	9.6	NSTAP	1.19
3	463	3.36	14.5	0.54	10360	0.18	28.8	0.06	9.6	NSTAP	0.86
4	758	2.05	8.9	0.33	10350	0.18	28.8	0.06	9.6	NSTAP	0.52
5	2154	0.72	3.1	0.11	10280	0.18	28.6	0.06	9.5	NSTAP	0.18

Table 4 Experimental parameters for the 5 matched cases for CTA2 and NSTAP probe for $z^+ \approx 29$ experiment

it of very high frequency and high gains, one would expect the amplifier to act as a filter. However, it is puzzling here that with only moderate gain the filtering becomes noticeable at such low frequencies. For typical instrument amplifiers with a gain-bandwidth product of say O(10MHz) and a gain of 15, one would not expect to attenuate signals until $f \gtrapprox 500$kHz.

4.4 NSTAP (with CTA2)

The final set of tests explore the temporal response of the Princeton NSTAP probe. This is a subminiature probe with a 100nm $\times$ 2μm $\times$ 60μm platinum sensing element, constructed using semiconductor and MEMS manufacturing techniques (for full details see Kunkel et al, 2006; Bailey et al, 2010; Vallikivi et al, 2011). Experimental conditions are given in table 4. The important detail to notice here is that the sensor length l is almost an order of magnitude smaller than the standard probes used in preceding tests. Figure 8(a) shows the calculated transfer function χ_e for the NSTAP experiments. The temporal response of the NSTAP/CTA2 system is much different, and much improved, compared to the same system operating standard probes. There is still a region of attenuation in the approximate range $500 < f_e < 5000$ Hz. Beyond $f_e \approx 5$kHz, there is a region of over amplification. However, the increase of this amplification with increasing f_e is much more gradual than for other probe types. As a comparison, figure 9 plots the average χ_e (for $e = 1-4$) versus f_e for the standard probe (gray) and the NSTAP probe (black) both operating with CTA2. From this comparison, it is clear that the over-amplification occurring for $f_e > 5$kHz is much more gradual and much less severe for the NSTAP probe. It should be noted that the standard probe was tested at $z^+ \approx 80$ and the NSTAP was tested at $z^+ \approx 29$, and also the square-wave response could not be tuned exactly the same, and so figure 9 is not quite a direct comparison of the two probe types. It is also noted that in neither case was the system optimally tuned, and thus there is ambiguity regarding what would be the best possible response that could be obtained from each system. However, in general figure 9 offers a clear indication of the extra temporal performance that can be gained with a given system by miniaturizing the sensor.

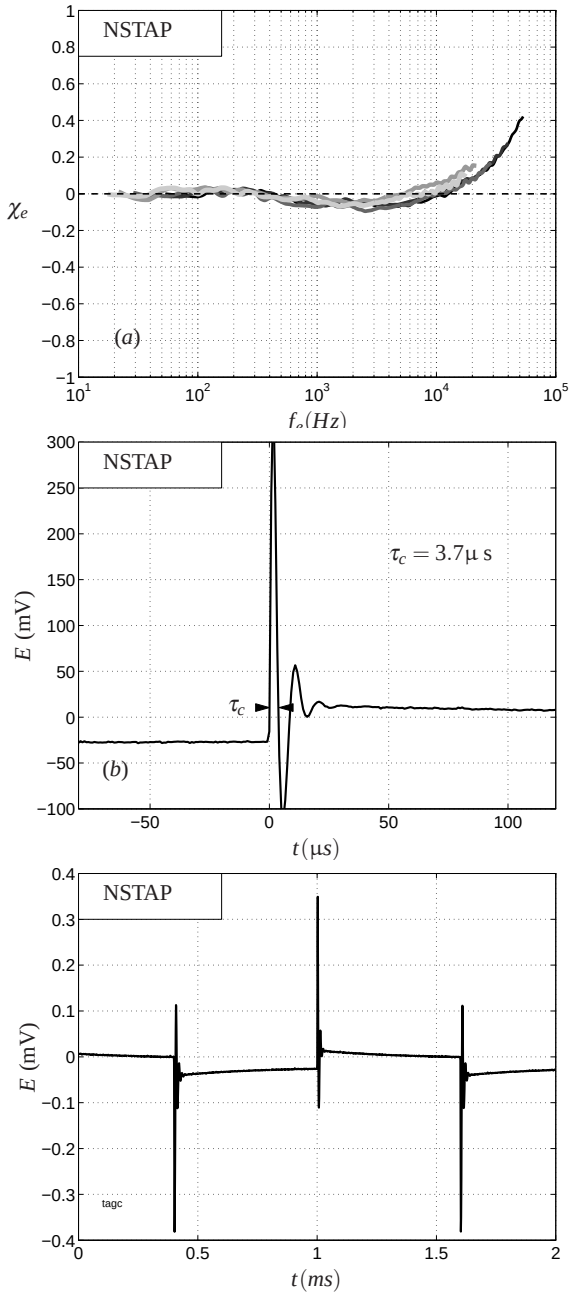


Fig. 8 (a) The difference function χ_e for the NSTAP probe and CTA2 at $z^+ \approx 29$. Line shading indicates centerline velocity from light (lowest U_0, $e = 5$) to dark (highest U_0, $e = 1$). (b) the corresponding square-wave response (c) expanded view of the square-wave response.

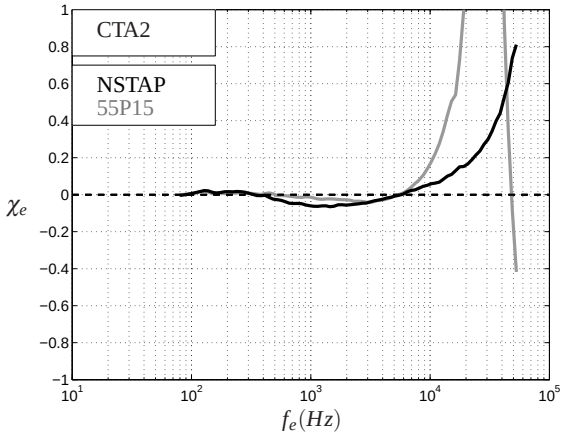


Fig. 9 Comparison of the transfer function χ_e for the same anemometer, but different probes (gray) standard probe at $z^+ \approx 80$ (black) N-STAP at $z^+ \approx 29$.

Figure 8(b) shows the sampled square-wave response test for the NSTAP experiment. Comparing this plot with figure 5 reveals that, for these under-damped cases, the N-STAP sensor yields a faster response. The timed decay of the initial step input $\tau_c = 3.7$ μs for the NSTAP sensor. Based on this value, equation (1), suggests a -3dB drop-off of 200 kHz. This is beyond the frequency at which we can accurately determine χ_e, however figure 8(a) does suggest that $\chi_e < -0.5$ will occur well beyond 50 kHz (although it should be noted that there will be growing error due to under-damped resonant type behaviour for $f \gtrsim 20$ kHz). Unfortunately it is not possible to plot the normalised energy spectrum of this square-wave response on figure 8(a) for comparison with the χ_e curve. The square-wave response measured for CTA2 with the NSTAP probe exhibits a very unusual higher-order response. This is clear by viewing a longer time history of the square-wave response as shown in figure 8(c). The gradual decay occurring after each step input over a time-scale of approximately 0.5 ms gives a nonsensical Bode plot.

5 What does this mean to the accuracy of measurements in wall-bounded turbulence?

Figure 10(a) collates all experimentally determined transfer functions χ_e onto a single plot. Each coloured curve shows the average response[3] for a particular system and set of conditions as detailed in the key. If we combine these curves with a known energy spectrum from a wall-bounded turbulent flow, it is possible to make predictions of the overall attenuation due to frequency response. For this we make use of the hot-wire measurements reported in Hutchins et al (2009) for a flat-plate zero-pressure-gradient turbulent boundary layer at $Re_\tau \approx 7300$. Since the freestream velocity for these measurements was only 10 ms^{-1}, we do not expect any major temporal resolution error for these original data. We will refer to these original results using subscript o. At each of 53 wall-normal measurement locations (logarithmically spaced from $8 < z^+ < 1.4Re_\tau$) we can produce an energy spectrum ϕ_{uu} as a function of frequency f_o for these original data. A new boundary layer (denoted with subscript n) with the same Reynolds number but an increased freestream velocity U_∞ will have turbulent energy shifted to higher frequencies in Hz (see figure 3 for example). Yet, assuming Reynolds number similarity, the original and the new pre-multiplied energy spectra will collapse when scaled with viscous variables (f^+ vs $k_x\phi^+_{uu}$). More precisely, since the ratio $\left|u_\tau^2/\nu\right|_o$ for the original experiment is known, it is possible to predict the frequency content of the spectrum at some 'new' value of this ratio $\left|u_\tau^2/\nu\right|_n$ using,

$$f_n = f_o \left|\frac{\nu}{u_\tau^2}\right|_o \left|\frac{u_\tau^2}{\nu}\right|_n \tag{7}$$

These predicted unattenuated energy spectra at $z^+ = 15$ are shown by the black curves in figures 10($b-d$) for $U_\tau^2/\nu \times 10^{-5}$ ratios of 0.305, 1.905 and 6.172 s^{-1} respectively. For unpressurised facilities where the working fluid is air (assuming $\nu \approx 1.5 \times 10^{-5}$ m^2 s^{-1}), these ratios correspond to freestream velocities of approximately 20, 50 and 90 ms^{-1}. We will denote this unpressurised equivalent freestream velocity as $U_{\infty_{sa}}$. Combining these energy spectra with the transfer functions shown in figure 10(a) enables us to predict the spectra (ϕ_{uu_p}) that would actually be measured by each of the anemometer configurations.

$$\phi_{uu_p}(f_n) = \phi_{uu_n}(f_n)\,[1 + \chi_e(f_n)] \tag{8}$$

It should be emphasized that these predicted spectra are valid only for the particular anemometer set-up employed here. A different user, with different settings would obtain a different performance. Nonetheless this analysis can serve as a useful indication of the likely errors due to heavily over- or under-damped systems. For figure 10(b), which shows a case where $U_{\infty_{sa}} \approx 20$ ms^{-1}, the error for each of the anemometer configurations is minimal. At these conditions, the majority of turbulent energy is contained within a frequency range where plot (a) indicates the transfer functions are relatively flat, and hence there is little sign of attenuation due to frequency response. However, as the ratio U_τ^2/ν increases, the turbulent energy is increasingly shifted to the right of plots (c) and (d) into a frequency range where the anemometer configurations studied here will attenuate or over-represent energy. For plot (c) where $U_\tau^2/\nu = 1.905 \times 10^5$ s^{-1}, corresponding to an unpressurised

[3] These average response curves are the mean of the χ_e verses f_e profiles determined for experiments $e = 1 \rightarrow 4$.

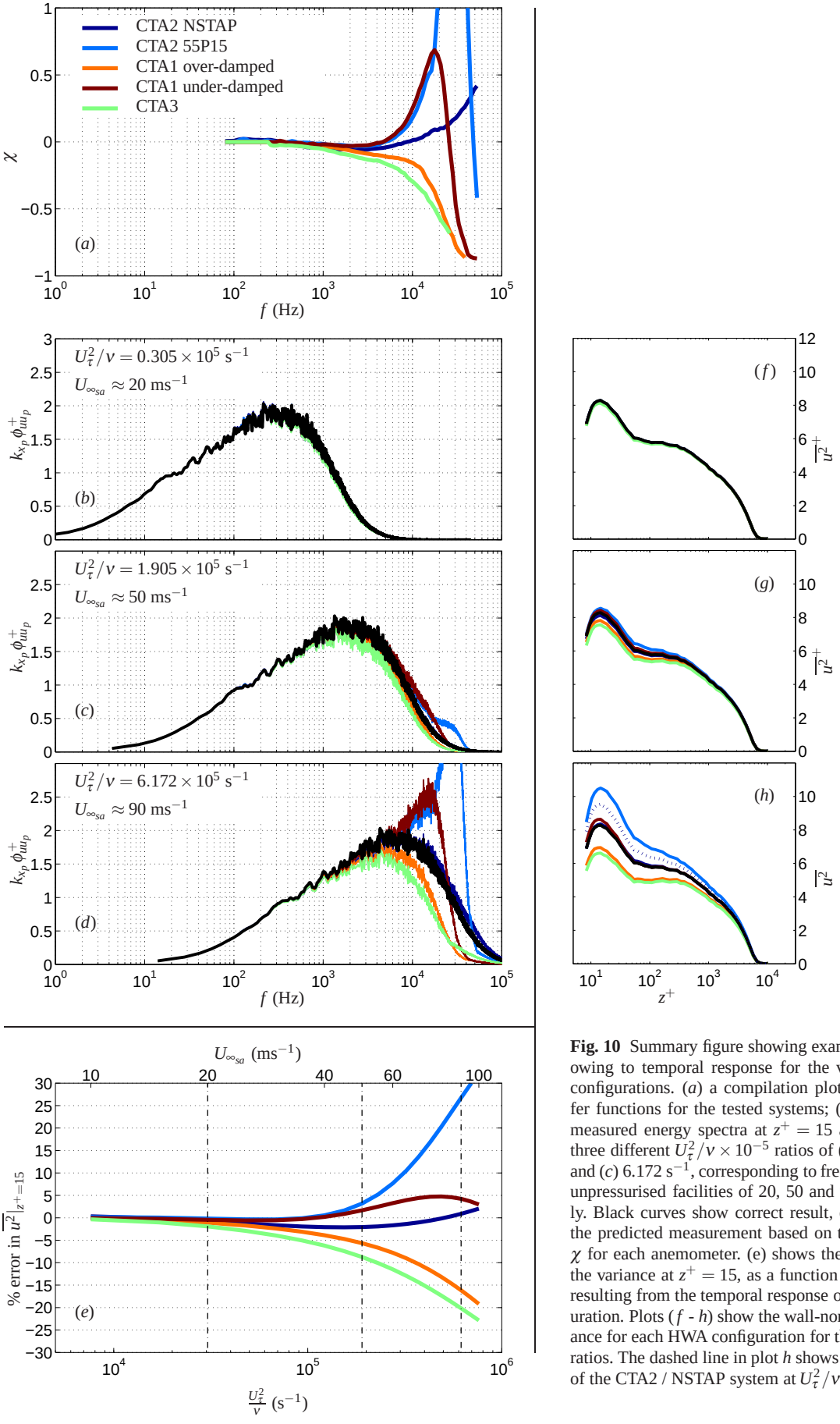


Fig. 10 Summary figure showing example expected errors owing to temporal response for the various tested HWA configurations. (*a*) a compilation plot showing the transfer functions for the tested systems; (*b* - *d*) the predicted measured energy spectra at $z^+ = 15$ and $Re_\tau \approx 7000$ for three different $U_\tau^2/\nu \times 10^{-5}$ ratios of (*a*) 0.305 , (*b*) 1.905 and (*c*) 6.172 s^{-1}, corresponding to freestream velocities in unpressurised facilities of 20, 50 and 90 ms^{-1} respectively. Black curves show correct result, coloured lines show the predicted measurement based on the transfer function χ for each anemometer. (e) shows the percentage error in the variance at $z^+ = 15$, as a function of U_τ^2/ν (and $U_{\infty_{sa}}$) resulting from the temporal response of each HWA configuration. Plots (*f* - *h*) show the wall-normal profiles of variance for each HWA configuration for the three $U_\tau^2/\nu \times 10^5$ ratios. The dashed line in plot *h* shows predicted behaviour of the CTA2 / NSTAP system at $U_\tau^2/\nu \approx 35 \times 10^5$ s^{-1}.

freestream velocity of approximately 50 ms^{-1}, we can begin to see differences developing in the spectra measured by each of the HWA configurations. In this case, these differences are most pronounced for the over-damped systems. For plot (*d*), where $U_\tau^2/\nu = 6.172\times10^5$ s^{-1}, corresponding to an unpressurised freestream velocity of approximately 90 ms^{-1}, the effect of frequency response is becoming acute for almost all systems tested (other than the NSTAP / CTA2 combination). Note that for these conditions, the heavily under-damped system (the standard 55P15 probe and CTA2) gives the largest error in spectra for all systems (giving a bigger error than CTA3 and over-damped CTA1). This is caused by the under-damped response and large resonant peak in the transfer function centered at $f \approx 31$ kHz. For this U_τ^2/ν ratio, substantial turbulent energy is located in this problematic frequency range leading to the large errors evident in figure 10 (*d*, *e* & *h*).

Figure 10(*e*) shows the percentage error in variance at $z^+ = 15$ corresponding to these predicted spectra as a function of U_τ^2/ν (lower abscissa) and unpressurised U_∞ (upper abscissa),

$$\%\text{ error in } \overline{u^2} = 100\times\frac{(\overline{u^2})_p - (\overline{u^2})_n}{(\overline{u^2})_n}$$

where,

$$(\overline{u^2})_p = \int (1+\chi_e)\phi_{uu_n} dk_{x_n}, \qquad (\overline{u^2})_n = \int \phi_{uu_n} dk_{x_n}$$

This could be a useful plot for experimentalists wishing to consider likely errors in experiments due to the frequency response of anemometer/probe system. Note that for $U_\tau^2/\nu \lessapprox 0.3\times10^5$ s^{-1} ($U_{\infty_{sa}} \lessapprox 20$ ms^{-1}) the errors in variance at $z^+ = 15$ are minimal for all systems. However, as U_τ^2/ν increases the errors become more severe. For an unpressurised freestream velocity of 90 ms^{-1} in air, we would expect $\sim 20\%$ attenuation of the variance measured by the over-damped systems, switching to a 25% over representation for the highly under-damped system (CTA2 with standard probe). It should be noted that although plot (*e*) indicates that the error in variance for the under-damped CTA1 appears to be small at $U_{\infty_{sa}} = 90$ ms^{-1}, this should really just be considered an anomaly. The spectra in plot (*d*) are greatly distorted, but in a manner in which the attenuation approximately counter-acts the over-representation. The time signal measured by this system would have significant errors for this U_τ^2/ν ratio.

Figure 10 ($f-h$) extends the view from the near-wall, to consider the error due to frequency response across the entire layer. As U_τ^2/ν increases, the anemometer systems give increasingly inaccurate representations of the mean variance profile. The exception here is the NSTAP / CTA2 combination which works remarkable accurately up to $U_\tau^2/\nu = 6.172\times10^5$ s^{-1}. Even so, it should be noted that this system is not immune to errors. The NSTAP has been designed for use in the Princeton Superpipe, a pressurised facility. At very high Reynolds numbers it is still conceivable that the ratio U_τ^2/ν will become large. For example, at a Reynolds number of $Re_\tau = 734\,000$ as reported by Zagarola (1996) the ratio $U_\tau^2/\nu \approx 35\times10^5$ s^{-1}. The dotted line in figure 10(*h*) shows the predicted profile for the CTA2 / NSTAP configuration at this ratio. In considering this result, it should be noted that to-date the NSTAP has not been operated above $Re_\tau \approx 100\,000$ due to limitations in structural strength.

There are several approximations involved in the creation of figure 10. The data of Hutchins et al (2009) contains an inherent attenuation owing to the finite size of the sensing element ($l^+ = 22$). Also, the analysis is strictly only valid at the Reynolds number of the original data ($Re_\tau = 7300$). As Reynolds number increases, an increasing proportion of the broadband energy is due to large outer-scaled turbulent events. This would lead to slight reductions in the percentage errors presented in figure 10(*e*). Such effects are a weak (logarithmic) function of Reynolds number (see Hutchins et al, 2009). In creating plots (*b*-*h*), the same transfer function χ is assumed for all wall-normal locations. In reality, χ will be a function of the local mean velocity and hence wall-normal location (z), with behaviour becoming increasingly damped close to the wall (refer to Appendix A). In spite of these limitations, this analysis can provide a useful estimate of the errors arising from frequency response for HWA measurements in high Reynolds number wall-bounded turbulence. In general HWA users should be cautious of flows that have substantial turbulent energy above the flat region of the response curves shown in figure 10(*a*).

6 Conclusions

A novel direct method for testing the frequency response of hot-wire anemometers to velocity fluctuations has been proposed and tested. This method is shown to provide a consistent and reliable estimate of the transfer function arising from the temporal response of the anemometry system. Several HWA systems with differing configurations have been tested and the implications of the determined frequency response to the accuracy of measurements in wall-bounded turbulence is considered. Based on these findings we can draw the following conclusions and recommendations,

(i) In flows where there is significant energy content beyond $5-7$ kHz, the frequency response of HWA systems can potentially cause large measurement errors in turbulence quantities.

(ii) For wall-bounded turbulence, a convenient parameter to judge frequency content is the ratio U_τ^2/ν. The

higher this ratio is, the higher the frequency content of the turbulent energy.

  - For $U_\tau^2/\nu \lessapprox 0.3\times10^5$ s^{-1} error due to frequency response will be minimal. This seems to be true for the three systems tested, regardless of whether the system is over- or under-damped.

  - For $U_\tau^2/\nu \gtrapprox 2\times10^5$ s^{-1} errors due to frequency response become significant (for $U_\tau^2/\nu \approx 6\times10^5$ s^{-1} misrepresentation of energy can exceed plus or minus 20% for heavily over- and under-damped systems respectively).

(iii) For CTA1 and CTA2 the energy spectrum of the square-wave response gives a reasonably good indication of the true response of the system, at least indicating over- or under-damped behaviour, and showing the location of any resonant peaks. The exception to this is CTA3, which has an electrical response that seems at odds with the measured response of the system. This variability unfortunately suggests that the high frequency performance of each anemometer must be carefully and directly ascertained (through non-electronic means, such as the method detailed here) prior to reliable high-frequency measurements.

(iv) The standard -3dB drop-off can be misleading. Caution should be exercised when interpreting the square-wave response. The standard -3dB drop-off (as estimated using equation 1) is an overly liberal estimate of the upper limiting frequency f_c for accurate boundary layer measurements (since -3dB represents a 50% attenuation in measured energy). For under-damped systems, there is a substantial error due to over-representation of the turbulent energy at frequencies approximately a decade lower than f_c determined in this manner (under-damped systems will exhibit attenuation in this frequency range).

(v) The response should be carefully checked across the expected range of operating conditions. For systems with behaviour similar to CTA1 and CTA2, viewing the energy spectrum of the square-wave response in real time whilst tuning the response of the anemometer might be the most promising method for attaining a flat response. Figure 3 demonstrates that changes in the square-wave response that can outwardly appear quite minor, can indicate a profound shift from over- to under-damped behaviour. Consequently, HWA systems that are 'optimally' tuned in the freestream, might be over-damped close to the surface of a wall-bounded turbulent flow. (See Appendix B).

(vi) Smaller sensing elements help. Preliminary measurements indicate that, when operated in an under-damped configuration, CTA2 with the NSTAP probe has an improved frequency response as compared to the same under-damped system with a standard probe geometry. Though these two experiments cannot be considered directly comparable, the results suggests that miniaturized sensors could hold a great promise for improved HWA measurements in high frequency flows.

A Variation of response within a boundary layer

Figure 11(a) shows the square-wave response measured in the freestream of a boundary layer wind-tunnel (the Melbourne HRNBLWT) at various mean velocities $\overline{U} = 10$, 3 and 1 ms^{-1} (black, red and blue curves respectively). The HWA system consists of CTA1 and a standard 55P15 probe. The anemometer has not been adjusted between these experiments and thus any difference between the three curves in Figure 11 is purely a result of the altered mean velocity. Figure 11(b) shows the corresponding normalised energy spectrum of the square-wave response, which for CTA1 is shown to give a reasonable representation of the *directly* determined response χ (see figure 3). The variation in mean velocity over the sensor causes a pronounced change in the measured response, shifting from an under-damped system at 10 ms^{-1} to a clear over-damped behaviour at 1 ms^{-1}. Such behaviour is to be expected from the heat transfer equation. As $\overline{U}$ reduces from 10 to 1 ms^{-1}, the wire Reynolds number has been decreased by a factor of approximately 10 reducing the heat transfer or cooling from the wire by a factor of approximately 3. Reduced heat transfer leads to increased damping. This is evident in Figure 11 with the system switching from under- to over-damped behaviour as the mean velocity reduces.

Figure 11 suggests that it is essential to check the square-wave response across the entire expected velocity range prior to a boundary layer traverse experiment. If the frequency response is only checked at freestream conditions (say 10 ms^{-1}), a system could encounter substantial temporal resolution issues close to the wall as the system becomes increasingly damped. For a wall-bounded turbulent flow with a freestream velocity of 10 ms^{-1}, local mean velocities of 3 and 1 ms^{-1} would be encountered at $z^+ \approx 10$ and 3. Hence the temporal response of the system would shift from under-damped to over-damped as the probe was traversed very close to the surface.

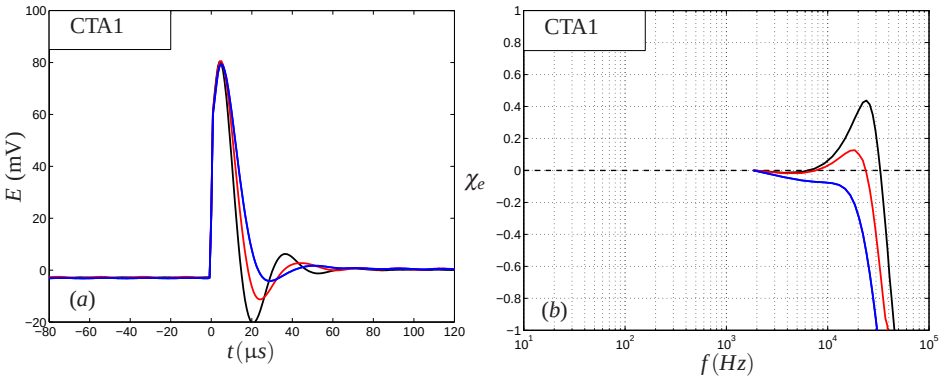


Fig. 11 The change with local mean velocity of (*a*) the square-wave response and (*b*) the normalised energy spectrum of the square-wave response. (black) $\overline{U} = 10.7$ ms^{-1}; (red) $\overline{U} = 3.5$ ms^{-1}; (blue) $\overline{U} = 1.0$ ms^{-1}. Tuning of anemometer has not been altered (changes are due only to the change in $\overline{U}$).

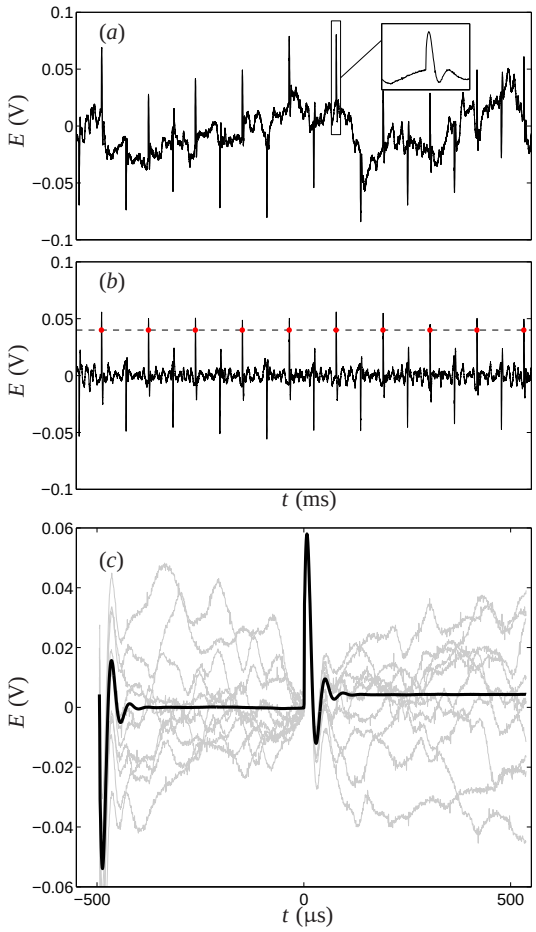


Fig. 12 Plots illustrating the extraction of the square-wave response from a turbulent signal measured in the core. (*a*) original time-series of the velocity output from the anemometer (sampled at 1.2 MHz) showing square-wave response superimposed onto turbulent signal, inset shows an expanded detail of the response to rising step function; (*b*) data high-pass filtered at 7kHz, dashed line shows detection threshold, red dots show rising edge detection; (*c*) ensemble average of detected rising edge step responses, gray lines show the individual detections shown in plots *a* and *b*, black curve shows ensemble average over 10s of data (approximately 10,000 individual occurrences).

B Determining the square wave response

The square-wave responses shown throughout this investigation were obtained with the probe at the pipe centerline, with the centerline velocity and pressurisation matched to the local conditions at the probe location (which was either $z^+ = 29$ or 80) for the baseline experiment *e*5. Since the pipe core is fully turbulent, the injected square-wave response is superimposed over a turbulent signal. For analysis, the signal is sampled at 1.2 MHz for a duration of 10 s. An example of this sampled signal for the under-damped CTA1 (as detailed in figures 1 - 3) is shown in figure 12(*a*), with an inset showing an enhanced detail of the square-wave response superimposed onto the turbulent core flow. To separate the square-wave response from the turbulent signal, the sampled data are filtered using a sharp spectral high-pass filter at $f = 7$kHz. An example of the resulting filtered signal is shown in figure 12(*b*). Note that the cut-off filter was selected to remove the large-scale turbulent component from the signal. A simple threshold technique is used to extract the square wave response. In the case shown, a threshold of 0.04 V was used detect the rising edge of the square wave input. Regions where the rising part of the signal exceeded this threshold are shown by the dot symbols on figure 12(*b*). A region of the signal surrounding this threshold crossing is then extracted and added to an ensemble average as shown in figure 12(*c*). The gray curves show the square-wave responses extracted from figure 12(*b*). The black curve shows the average response.

Acknowledgements NH and JPM were supported under the Australian Research Council's Discovery Projects (project number DP110102448) and Future Fellowship funding schemes (project numbers FT110100432 and FT120100409). AJS was supported through ONR Grant N00014-13-1-0174.

References

Ashok A, Bailey S, Hultmark M, Smits A (2012) Hot-wire spatial resolution effects in measurements of grid-generated turbulence. Experiments in Fluids 53(6):1713–1722, DOI 10.1007/s00348-012-1382-5

Bailey SC, Kunkel GJ, Hultmark M, Vallikivi M, Hill JP, Meyer KA, Tsay C, Arnold CB, Smits AJ (2010) Turbulence measurements using a nanoscale thermal anemometry probe. J Fluid Mech 663:160–179

Bonnet JP, de Roquefort TA (1980) Determination and optimization of frequency response of constant temperature hot-wire anemometers in supersonic flows. Rev Sci Instrum 51:234–239

Bruun HH (1995) Hot-wire anemometry. Oxford University Press

Chin CC, Hutchins N, Ooi ASH, Marusic I (2009) Use of direct numerical simulation (dns) data to investigate spatial resolution issues in measurements of wall-bounded turbulence. Meas Sci Technol 20(11):115,401

Chin CC, Hutchins N, Ooi A, Marusic I (2011) Spatial resolution correction for hot-wire anemometry in wall turbulence. Exp Fluids 50:1443–1453

Comte-Bellot G (1976) Hot-wire anemometry. Annu Rev Fluid Mech 8:209–231

Fernholz HH, Krausse E, Nockermann M, Schober M (1995) Comparative measurementsin the canonical boundary layer at $Re_{\delta_2} \leqslant 6 \times 10^4$ on the wall of the German-Dutch windtunnel. Phys Fluids 7(6):12751281

Freymuth P (1967) Feedback control theory for constant-temperature hot-wire anemometers. Rev Sci Instrum 38(5):677–681

Freymuth P (1977) Frequency response and electronic testing for constant-temperature hot-wire anemometers. J Phys E: Sci Instrum 10(7):705–710

Hites MH (1997) Scaling of high-Reynolds number turbulent boundary layers in the National Diagnostic Facility. PhD thesis, Illinois Institute of Technology, Chicago

Hutchins N, Nickels TB, Marusic I, Chong MS (2009) Hot-wire spatial resolution issues in wall-bounded turbulence. J Fluid Mech 635:103–136

Khoo BC, Chew YT, Li GL (1995) A new method by which to determine the dynamic response of marginally elevated hot-wire anemometer probes for near-wall velocity and shear stress measurements. Meas Sci Technol 6:1399–1406

Kidron I (1966) Measurement of the transfer function of hot-wire and hot-film turbulence transducers. IEEE T Instrum Meas 15:76–81

Ko NWM, Ho KK (1977) On the determination of frequency response of hot-wire system. IEEE T on Instrum and Meas 26(4):360–367

Kunkel GJ, Arnold CB, Smits AJ (2006) Developement of NSTAP: Nanoscale thermal anemometry probe. AIAA-paper 2006-3718

Li JD, Mckeon BJ, Jiang W, Morrison JF, Smits AJ (2004) The response of hot wires in high Reynolds-number turbulent pipe flow. Meas Sci Technol 15:789–798

Ligrani PM, Bradshaw P (1987) Spatial resolution and measurement of turbulence in the viscous sublayer using subminiature hot-wire probes. Exp Fluids 5:407–417

Monkewitz PA, Duncan RD, Nagib HM (2010) Correcting hot-wire measurements of stream-wise turbulence intensity in boundary layers. Phys Fluids 22:091,701

Morrison JF, McKeon BJ, Jiang W, Smits AJ (2004) Scaling of the streamwise velocity component in turbulent pipe flow. J Fluid Mech 508:99–131

Nickels TB, Marusic I, Hafez S, Hutchins N, Chong MS (2007) Some predictions of the attached eddy model for a high Reynolds number boundary layer. Phil Trans R Soc A 365:807–822

Örlü R, Alfredsson PH (2010) On spatial resolution issues related to time-averaged quantities using hot-wire anemometry. Exp Fluids 49:101–110

Österlund JM (1999) Experimental studies of zero pressure-gradient turbulent boundary-layer flow. PhD thesis, Department of Mechanics, Royal Institute of Technology, Stockholm

Oxlade AR, Valente PC, Ganapathisubramani B, Morrison JF (2012) Denoising of time-resolved piv for accurate measurement of turbulence spectra and reduced error in derivatives. Exp Fluids 53:1561–1575

Perry AE, Li JD (1990) Experimental support for the attached-eddy hypothesis in zero-pressure-gradient turbulent boundary layers. J Fluid Mech 218:405–438

Perry AE, Morrison GL (1970) Static and dynamic calibrations of constant temperature hot-wire systems. J Fluid Mech 47:765–777

Segalini A, Cimarelli A, Rüedi JD, Angelis ED, Talamelli A (2011a) Effect of the spatial filtering and alignment error of hot-wire probes in a wall-bounded turbulent flow. Meas Sci Technol 22(10):105,408

Segalini A, Örlü R, Schlatter P, Alfredsson PH, Rüedi JD, Talamelli A (2011b) A method to estimate turbulence intensity and transverse taylor microscale in turbulent flows from spatially averaged hot-wire data. Exp Fluids 51:693–700

Smits AJ, Zagarola MV (2005) Applications of dense gases to model testing for aeronautical and hydrodynamic applications. Meas Sci Technol 16:1710–1715

Smits AJ, Monty JP, Hultmark M, Bailey SC, Hutchins N, Marusic I (2011) Spatial resolution correction for wall-bounded turbulence measurements. J Fluid Mech

Talamelli A, Persiani F, Fransson JHM, Alfredsson PH, Johansson AV, Nagib HM, Rüedi JD, Sreenivasan KR,

Monkewitz PA (2009) CICLoPE - a response to the need for high reynolds number experiments. Fluid Dyn Res 41(2):021,407, DOI 10.1017/S0022112089002892

Valente PC, Vassilicos JC (2011) Comment on “dissipation and decay of fractal-generated turbulence”. Phys Fluids 23:119,101

Vallikivi M, Hultmark M, Bailey S, Smits A (2011) Turbulence measurements in pipe flow using a nano-scale thermal anemometry probe. Experiments in Fluids 51(6):1521–1527

Watmuff JH (1995) An investigation of the constant-temperature hot-wire anemometer. Exp Therm and Fluid Sci 11(2):117 – 134

Weiss J, Knauss H, Wagner S (2001) Method for the determination of frequency response and signal to noise ratio for constant-temperature hot-wire anemometers. Rev Sci Instrum 72(3):1904–1909

Zagarola MV (1996) Mean flow scaling of turbulent pipe flow. PhD thesis, Department of Mechanical and Aerospace Engineering, Princeton University, USA

Zagarola MV, Smits AJ (1998) Mean-flow scaling of turbulent pipe flow. J Fluid Mech 373:33–79